https://doi.org/10.5194/egusphere-2026-1629
Preprint. Discussion started: 22 May 2026

Effects of model resolution on predicting atmospheric ducting conditions with Harmonie-AROME

Karoliina Hämäläinen[1], Laura Rautiainen[1], Jani Tyynelä[1], and Lauri Laakso[1]
[1]Finnish Meteorological Institute, PL 503, 00101 Helsinki, Finland.
Correspondence: Karoliina Hämäläinen (karoliina.hamalainen@fmi.fi)

Abstract. To avoid hazardous situations, it is important to be able to forecast the condition leading to anomalous propagation of electromagnetic signal. In this study, the operational weather forecasting model Harmonie-AROME used by the Finnish meteorological institute was utilized to assess the effects of model resolution on predicting atmospheric ducting conditions. Four separate model configurations were tested altering the vertical and horizontal resolution. The testing period (from 19th of June to 12th of July, 2022) included several occasions when anomalous propagation had been detected at Northern Baltic sea by the Utö coastal surveillance radar. The comparison against the observations show potential of predicting ducting conditions with numerical weather prediction model. At the same time the results reveal the limitations of the model in producing realistic vertical profiles of temperature and humidity especially near surface.

1 Introduction

Modern society relies on telecommunication and different radar applications, both on civil and military sector. In this context, aviation and marine traffic are especially vulnerable to disturbances. Certain weather conditions can cause anomalous signal propagation of the electromagnetic waves leading to interference in radar applications and radio communication. During such conditions the signal gets trapped into a shallow horizontal layer. This phenomena is commonly called as ducting (Turton et al., 1988).

Atmospheric ducting cannot be measured directly; however, its presence can be detected through its impact on electromagnetic signal propagation. One clear indicator is the anomalous extension of radar coverage under certain meteorological conditions (Norin et al., 2023; Norin, 2022). In such cases, targets located well beyond the normal radar horizon can become detectable (Patterson and Skolnik, 2008). This occurs when the radar signal becomes trapped within a quasi-horizontal refractive layer in the atmosphere, allowing it to propagate over extended distances with reduced attenuation.

Ducting conditions can also be detected using a transmitter–receiver pair to determine the presence and strength of a received signal (Grabner and Kvicera, 2003; Rautiainen et al., 2025). Fixed radio transmission infrastructure, such as radio towers, can

https://doi.org/10.5194/egusphere-2026-1629
Preprint. Discussion started: 22 May 2026

serve as monitoring points for observing instances of unexpected long-range signal propagation, thus providing empirical evidence of ducting.

The electromagnetic signal propagation characteristics depend on meteorological conditions (Turton et al., 1988). The vertical stratification of air temperature and humidity are the main properties affecting atmospheric refractivity, and thus signal propagation. Weather events involving strong turbulent mixing, such as wind and precipitation, prevent the evolution of such stratification. While, evaporation, subsidence, advection, and nocturnal radiative cooling are known as meteorological conditions leading to the existence of ducts. In addition, temperature stratification caused by sea surface conditions plays a critical role. For example, cold seas can create stable atmospheric layers, while warm seas nourish instability. Seasonal variations between winter and summer have an effect on heat fluxes and thermal stratification. Over ice-covered surfaces, ducting can occur due to a sharp thermal stratification.

Often the duct types are divided into four categories depending on how the duct is formed (Derksen, 2016; Babin et al., 1997; Mai et al., 2020): surface duct, surface-based duct, elevated duct and evaporation duct. Surface and surface-based ducts form due to temperature inversion and/or hydrolapse which causes a decrease in refractivity. The meteorological conditions leading to inversion are advection, subsidence near high pressure system or cold fronts, or radiative night time cooling, or cold sea surface. Surface ducts are more common on sea areas (Turton et al., 1988). Elevated ducts have similar structure as surface ducts, but the ducts are not connected to the surface. Elevated ducts are formed near subsidence areas or due to uplift of the air near frontal systems. The evaporation duct occur when a strong humidity gradient develops, caused by rapid evaporation from the warm sea surface into cooler, drier air above. This moist air affect on the refractive properties of the atmosphere, creating a ducting layer that can trap the radio waves. The factors influencing on evaporation duct formation include: 1) high sea surface temperatures, 2) stable atmospheric conditions, 3) light to moderate winds.

Traditionally, propagation models get their initial conditions from in-situ observations such as radiosonde soundings (Wagner, 1960; Ao, 2007). These observations are accurate at the site, but do not represent wider atmosphere and do not give indication of the possible situation after few hours or days. To be able to utilize these propagation models in forecasting of future conditions, they need to be coupled with a weather prediction model such as Haack et al. (2010); Pastore et al. (2021) have tested. But how well do the weather prediction models meet the needs of the propagation models? Are the weather prediction models able to generate reasonable enough vertical structures of temperature and humidity?

In this study, the effects of NWP (Numerical Weather Prediction) model Harmonie-AROME (Bengtsson et al., 2017), resolution (both horizontal and vertical) on forecasted modified refractivity gradient is studied. The modeled vertical profiles of modified refractivity, specific humidity and air temperature are compared against the mast measurements carried out at Utö atmospheric and marine research station (Laakso et al., 2018; Rautiainen et al., 2023a). The aim of this study is to enhance the understanding on how well the NWP model can represent the ducting conditions (Von Engeln and Teixeira, 2004; Lopez, 2009; Norin et al., 2023) in a marine environment (Förster and Riechen, 2006; Essen et al., 2012; Mesnard and Sauvageot, 2010; Norin, 2022; Rautiainen et al., 2025).

https://doi.org/10.5194/egusphere-2026-1629
Preprint. Discussion started: 22 May 2026

In this paper, in section 2 we present observations used for the model validation. Section 3 describes the post-processing methods and NWP model used in this study. Section 4 is dedicated to the results. Section 6 presents the conclusions based on the results and the final section 5, is dedicated to wider discussion and future plans.

2 Observations

In this study experimental data from different sources and different purposes is used. For NWP model data-assimilation we use a wide range of continuous meteorological observations. The data used include SYNOP, TEMP, soundings, lidar, weather radar, ceilometer and satellite observations, which are used in initialization of forecast runs through assimilation (Grønsleth and Randriamampianina, 2012; Hagelin et al., 2021; Barkmeijer et al., 2021).

NWP model simulations are compared with extensive field observations at Utö Atmospheric and Marine Research Station (see Fig. 1). The station and observations are described in detail in Laakso et al. (2018); Honkanen et al. (2018) and Rautiainen et al. (2023b, a). In this study we utilize vertical observations of air temperature and humidity from two measurements mast located approximately 500 m apart. T and RH are measured with Rotronik HC2A-S3 T-RH and Vaisala HMP155EC T-RH sensors installed at 4 m, 7 m, 12 m, 22 m, 32 m and 59 m heights above the mean sea level (amsl), allowing a very precise examination of the vertical structure of the atmosphere near the surface.

According to Rautiainen et al. (2025), ducting was frequently observed with the Utö coastal surveillance radar. Based on these analysis, we selected the period from 19 June to 11 July 2022 for NWP model simulations. Within this time frame, multiple ducting episodes occurred. The testing period was restricted to three weeks due to the computational cost of the NWP experiments.

3 Methods

3.1 Calculating Atmospheric Refractivity and possibility of Ducting

The prognostic values for atmospheric refractivity can be calculated based on NWP model output. The equation 1 (Turton et al., 1988) shows the semi-empirical formulation for refractivity N

$$N = \frac{77.6}{T}(p + 4810\frac{e}{T}) \tag{1}$$

in which the T is the air temperature [K], p is the air pressure [hPa], and e is the water vapor pressure [hPa]. The water vapor pressure is not a common output parameter of the NWP model, but it can be calculated through specific humidity q [unitless] (Babin et al., 1997; Bechtold, 2015):

$$q = \frac{e \cdot \epsilon}{p - (1 - \epsilon) \cdot e} \tag{2}$$

https://doi.org/10.5194/egusphere-2026-1629
Preprint. Discussion started: 22 May 2026

in which ϵ is a ratio of molar masses of vapor and dry air (0.622). From this equation the water vapor pressure can be derived:

$$e = \frac{p \cdot q}{\epsilon + (1 - \epsilon) \cdot q} \tag{3}$$

The best way to estimate signal propagation in the atmosphere is to use modified refractivity M (Turton et al., 1988), which can be calculated based on refractivity N. Modified refractivity takes into account the natural bending of the signal in the atmosphere due to curvature of the ground. In equation 4, the z is the height above the surface level and R is the mean radius of the earth.

$$M = N + \frac{z}{R} \cdot 10^6 \tag{4}$$

The vertical gradient of the M describes the behaviour of the signal propagation in the atmosphere. When modified refractivity decreases with height, the signal is strongly bent downwards. In contrast, when modified refractivity increases with height, the signal propagates nearly straight, while the Earth's curvature causes the surface to fall away beneath it at longer distances. Based on the strength and sign of the gradient the signal propagation can be divided into four categories (Turton et al., 1988): standard, sub-refractivity, super-refractivity and trapping. Depending on the elevation angle of the emitted radar beam, a signal that enters the duct at a sufficiently small incidence angle can become trapped within the layer, where it is repeatedly refracted and guided along the duct (Turton et al., 1988).

Based on the NWP model output, modified refractivity was calculated for each grid point, with one hour time interval. Next, the vertical gradient of modified refractivity was calculated and the duct types were computed. These calculations were executed for all four model experiments to compare how the changes in model resolution affect the forecast skill of ducting.

Based on Turton et al. (1988), the presence of hydrolapse and temperature inversion enhance the formation of a duct, while pressure changes are negligible. Yet, the effects of hydrolapse are more dominant. Based on the equation 1 we can draw conclusions on the expected strength of the duct. The simplified table 1, is presented here to help to understand the connections between the temperature and humidity. The amount of (+) signs indicate how strong duct can be expected to form in different weather conditions. Note, that the strength of the duct is due to the differences between the air masses on different levels. These variations affect how the electromagnetic signals propagate, causing stronger or weaker ducting conditions depending on the atmospheric conditions.

3.2 Weather model Harmonie-AROME

The current operational numerical weather prediction model used at FMI (Finnish Meteorological Institute) is Harmonie-AROME (Müller et al., 2017; Frogner et al., 2019). At the time this study took place the model version was cy43h2.2.1. The Harmonie-AROME is a meso-scale model suitable for convective permitting scales. It has non-hydrostatic dynamics (Bénard et al., 2010; Bubnová et al., 1995) with fully compressible Eulerian equations (Laprise, 1992; Simmons and Burridge, 1981). The equations are solved in time and space with a semi-Lagrangian advection scheme on a grid and a semi-Implicit two-time-level scheme following spectral representation of prognostic variables with double Fourier decomposition (ECMWF, 2015).

https://doi.org/10.5194/egusphere-2026-1629
Preprint. Discussion started: 22 May 2026

The model calculation step is 75 seconds, and the horizontal grid space is 2.5 km with 65 vertical levels (Bengtsson et al., 2017). Wherein, the lowest model level is approximately at 10 m height and the top is at 10 hPa (∼33 000m). The model physics parameterization schemes are described in more detailed in Bengtsson et al. (2017) and Seity et al. (2011).

In HARMONIE-AROME, each grid point consists of multiple surface tiles, and near-surface variables such as temperature (T2m) and specific humidity (Q2m) are computed as weighted averages over these tiles according to their fractional coverage. For each tile the diagnostic values are obtained by interpolating between lowest model level and surface (Geleyn, 1988; Dian and Masek, 2015).

The Harmonie-AROME is nested together with IFS forecasts from ECMWF (The European Centre for Medium-Range Weather Forecasts, ECMWF (2023)). IFS provides initial and boundary conditions for Harmonie-AROME, including the sea surface temperature (SST) analysis. This analysis originate from the OSTIA Sea Surface Temperature analysis provided by the UK Meteorological Office (Good et al., 2020). In the operational runs the SST is kept constant during the whole forecast cycle, which may cause forecasting error on near surface temperature in an upwelling situation.

In respect to radar refractivity, the most important parameterization scheme in Harmonie-AROME is the turbulence scheme HARATU (Van Meijgaard et al., 2012). The turbulence scheme affects air temperature and humidity, through cloud/fog formation and wind. The turbulent kinetic energy (TKE) has source and sink terms which take into account wind shear, buoyancy, transport and dissipation of TKE. The turbulent mixing length includes two parts: a stable conditions and near-neutral convective conditions (Lenderink and Holtslag, 2004). The stability coefficients take into account moist processes, such as cloud droplet condensation and evaporation and how these processes affect latent heat.

3.3 NWP experiments

In this study, four different model resolutions were tested to see how the vertical and horizontal resolution affects predictions of radar refractivity. These model configurations are presented in Table 2. The vertical resolution was tested with 65 and 90 levels. Similarly, the horizontal resolution was changed between 750 m and 2500 m. For all of the model configurations the forecast length was set to 24 h + analysis time, and cycled 4 times per day (00, 06, 12 and 18 UTC). The study area (fig.1) and period (19. June - 11. July, in 2022) were chosen based on available observations from the Utö mast and Utö coastal surveillance radar (Rautiainen et al., 2025).

The NWP model output was post-processed by using the equations presented in section (2). The values for modified refractivity were calculated and compared against the observation based values. The temperature and specific humidity profiles were also analyzed to widen the understanding of possible forecasting errors. The results of these calculations are presented in next section.

3.4 Verification metrics

Model performance was evaluated using standard categorical verification metrics derived from a 2 × 2 contingency table. Ducting conditions were defined in a binary framework (“Yes”/“No”) for both observations and forecasts using the modified refractivity gradient threshold dM/dh<0. The observational classification was based on mast measurements from which the

https://doi.org/10.5194/egusphere-2026-1629
Preprint. Discussion started: 22 May 2026

vertical gradient of modified refractivity was derived, as described in Section XX. This classification yields four possible outcomes: hits (both forecast and observed), false alarms (forecast only), misses (observed only), and correct rejections (neither forecast nor observed).

From these counts, a set of skill scores was calculated. The frequency bias (Bias) quantifies the ratio of forecast occurrences to observed occurrences, indicating underprediction (Bias < 1) or overprediction (Bias > 1), with an ideal value of 1. The proportion correct (PC) represents the fraction of all correctly classified cases, including both hits and correct rejections.

To emphasize the correct prediction of ducting events, the threat score (TS), also known as the critical success index, was used. TS measures the proportion of correctly forecast events relative to all cases where ducting was either forecast or observed, excluding correct rejections. The probability of detection (POD) describes the fraction of observed ducting events that were successfully forecast, whereas the false alarm ratio (FAR) represents the fraction of forecast events that did not occur. Since POD is insensitive to false alarms and FAR does not account for missed events, these metrics are interpreted together.

The resulting skill scores are summarized in the Performance diagram (fig. 8), where POD is plotted against the success ratio (1 - FAR). In this representation, points closer to the upper-right corner indicate better overall performance, combining high detection rates with low false alarm frequencies. Lines of constant frequency bias and threat score provide additional guidance for interpretation, allowing simultaneous assessment of forecast reliability and event detection capability.

4 Results

Analysis of vertical gradients from Utö mast observations, in figure 2, show separately the effects of temperature and water vapor pressure on the M-gradient. A positive temperature gradient with decreasing modified refractivity occurs in 8.6% of time during testing period, while a negative water vapor pressure gradient with decreasing modified refractivity is more frequent at $\sim$30 %. The combined condition of positive temperature and negative water vapor pressure gradients occurs in 8.6% of cases (not shown in fig), similar to the temperature-only condition. This, highlights the dominant role of moisture in generating negative M-gradients and conditions favorable for ducting.

Figure 3 represents time series of modified refractivity for the testing period. The first panel shows the calculated values based on the Utö mast measurements. The next four panels are model experiments with varying vertical and horizontal resolutions, with 65 - 90 levels and 750m - 2500m. The vertical axis is restricted to the NWP model levels that are comparable to the Utö measurements (lower than 60m). Therefore, only the lowest three levels are included in the figures for the L65 and four levels for the L90. Note, the M-gradient is the change between two levels. The bluish negative values indicate presence of ducting conditions.

The top panel of figure 3 shows, that during the test period ducting conditions were mostly occurring in a very shallow layer ($<$ 15m) above the ground. The following panels in this same figure, immediately reveal the limitations of the NWP model. None of the experiments are able to capture the near surface ducts (lower than 15m) correctly. However, the results in the upper level ($\sim$ 30m) show remarkably similar features compared to observations.

https://doi.org/10.5194/egusphere-2026-1629
Preprint. Discussion started: 22 May 2026

The first ducting situation around midnight of 22nd June 2022, was captured by all the NWP model configurations. In the experiments with L65 vertical resolution, the forecasted ducting conditions are expected to be much stronger compared to the observation. Yet, the experiments with L90 have a more realistic vertical structure. The gradient is not as strong near the surface during this event; however, this comes at the cost of temporal accuracy regarding the event's duration. Similar features are seen during the ducting event from 25th to 28th of June. A broader analysis of the weather maps (not shown here) reveal that the first event is related to a cold front passing over Utö islands. The longer ducting event during 26th - 28th June is related to a high pressure system over Estonia, leading to subsidence.

The time series of specific humidity is presented in figure 4. There is a hydrolapse (specific humidity decreasing with height) during the event on 22nd June 2022. Yet, the model is dryer than the observation. Also based on figure 4 (two upper most pannels), the model experiments are much colder than observed. Similar features also occur between 26th - 28th June and 2nd of July.

During the time period between 3rd - 10th of July strong ducting conditions are observed near the surface which the models are not able to replicate (fig. 3). The model experiments with L90 have a small guess about the event, but they are not able to form strong enough ducting conditions near the surface and the duration of the events are far too short. The vertical humidity structure is not strong enough in these cases. Overall, experiments with 750m horizontal resolution are able to capture the diurnal temperature cycle more accurately, compared to 2500m experiments (fig. 6). These events are also related to frontal activity, but much weaker occluded fronts.

In figure 5, scatter plots for temperature, specific humidity and modified refractivity are shown between the modeled and observed values for heights 2 m, 30 m and 60 m. A perfect forecast would land on the diagonal. Similar features were present in all the model configurations, thereby only our operational weather forecasting configuration (2500L65) is presented here. Based on this figure, the weather model under predicts high temperature (>22 °C) and water vapor pressure (>22 hPa) values, which leads to an underestimation of the magnitude of the modified refractivity. Importantly, as already shown the importance of moisture (fig. 2), too-low value near the surface reduces the likelihood of achieving a negative M-gradient. Yet, if the forecasting error is of equal size for the consecutive vertical levels, it does not have an effect on the M-gradient.

A detailed inspection of the tile distribution (see. section 3.2) at the Utö mast coordinates shows that, at 2500 m horizontal resolution, the grid point is classified as 100% sea. At higher resolution (750m) experiments, the same location is still mainly sea, with more than 80% sea fraction. This leads to a different surface energy balance compared to the actual measurement site, which is located on a small island. In particular, the higher heat capacity of water restrict the diurnal temperature cycle and limits daytime warming (fig. 6), resulting in a systematic cold bias during early summer.

At 30 m height, the observed diurnal cycle is no longer evident (even in measurements, fig. 4), yet the negative temperature bias persists. A similar increase in bias is also seen in specific humidity during this period, suggesting that the misrepresentation of surface conditions affects both temperature and moisture fields. In contrast, the model reproduces wind speed and direction at 30 m reasonably well, indicating that the large-scale flow is captured accurately, while near-surface thermodynamic processes remain poorly represented.

https://doi.org/10.5194/egusphere-2026-1629
Preprint. Discussion started: 22 May 2026

Figure 7 shows an example of profiles, and highlights the challenges the model faces in representing near-surface temperature inversions and humidity structures. Observations show a much sharper vertical gradient close to the surface than either of the model configurations, even though the total temperature and humidity difference between the surface and 30 meters height is similar. The limited number of vertical levels in the model leads to too linear representation of the profile compared to the observations, which benefit from a higher vertical resolution and therefore are able to capture more detailed structure in this shallow layer. Although the L90 experiment has a more realistic vertical structure of specific humidity, it is not able to capture the shallow temperature inversion correctly, leading to over-prediction of the M-value.

Figure 8 shows the performance diagram of modified refractivity for Utö station during the testing period. The probability of detection (POD) and success ratio (SR) are presented for each observation level and model experiment separately. The perfect forecast would land at the top right corner, having POD = 1 and SC = 1, with false alarm ratio = FAR = 0. At the lowest observation levels (5m and 10m), the probability of detection for negative modified refractivity gradient is only 47%. However, higher up (20m, 30m, 60m), the models exhibit significantly similar features to the observations, with prediction accuracies ranging from 91% to 97%. Overall, the false alarm ratio remains very modest, at approximately 6% to 10%. FAR is a ratio between correctly forecasted events and false alarms. FAR does not take into account missed events.

5 Discussion

The aim of this study was to evaluate the ability of the NWP model HARMONIE-AROME to forecast ducting by varying both horizontal and vertical resolution. Forecasts were compared to observations from the Utö mast. The results indicate that vertical resolution has a greater impact on forecast accuracy than horizontal resolution, particularly for near-surface temperature and humidity structures. In complex coastal and archipelago environments, such as the Finnish coastline, small-scale surface features may not be fully resolved at typical model grid resolutions. As demonstrated by the Utö case, this can locally influence the representation of near-surface conditions, even though the model performs well overall.

Signal propagation also depends on the relative position between the duct and the signal source: the closer the source is to the duct, the higher the likelihood of signal trapping. A dedicated propagation model is therefore required to calculate actual signal paths. Nevertheless, NWP refraction forecasts provide a useful overview of the location and height of potential ducts, allowing users to assess possible impacts based on their own position.

Future work includes exploring methods to artificially increase the number of diagnostic levels or the resolution of certain variables without the need to run the full 3D model at higher vertical resolution, which is computationally expensive. Such approaches may allow more detailed analyses of near-surface and boundary layer processes while keeping the operational model setup unchanged. In parallel, further improvements in vertical resolution could be considered, but diagnostic tools provide a cost-effective alternative to adding additional model levels.

If these developments are successful, ensemble forecasts of refractivity could be implemented, providing estimates of forecast uncertainty. As refractivity is highly sensitive to small vertical variations in temperature and humidity, enhancing forecasts of these parameters will directly improve the predictability of ducting conditions.

https://doi.org/10.5194/egusphere-2026-1629
Preprint. Discussion started: 22 May 2026

Overall, the results of this study support the plan to increase the number of vertical levels in the operational NWP model and to continue improving the representation of near-surface thermodynamic processes.

6 Conclusions

Although the model struggles to reproduce near-surface temperature inversions and humidity structures, at higher levels the forecasts are in closer agreement with observations. The grid point at Utö is largely sea, even at 750 m resolution, which limits daytime warming and the diurnal cycle near the surface. Consequently, due to the misrepresentation of the land–sea distribution at the measurement site, the model systematically underestimates near-surface temperature and humidity. Introducing more vertical levels improves the representation of gradients and adds structure to the forecasts, reflecting the sensitivity of modified refractivity to vertical changes in temperature and humidity.

Notably, at 30 m height the model and observations begin to resemble each other, and wind speed and direction are well captured. This indicates that, when surface effects are less dominant, the model has the potential to reproduce thermodynamics accurately. Overall, the study highlights the importance of resolving both vertical structure and heterogeneous coastal surfaces in high-resolution models to improve forecasts of temperature, humidity, and ducting conditions in marine and coastal environments.

Code and data availability.

The Harmonie-AROME model, developed collaboratively at the European level, is not publicly available, as it is built on the same code framework as the global ECMWF/IFS and MF/Arpege models. These global models are not open source and share a substantial portion of their code with Harmonie. Therefore the access is trestricted to ECMWF, Arpege, and ACCORD partners. Similarly, the raw data from the test period (spanning over three weeks and four experiments, approximately 5 T) cannot be fully shared due to its size. In our experiments, we used the NWP version `harmonie_release/git/tags/harmonie-43h2.2.1`, with modifications applied only to the Harmonie namelist variables related to resolution, as detailed here:

https://doi.org/10.5194/egusphere-2026-1629
Preprint. Discussion started: 22 May 2026


```
# In harmonie_exp/nam/config_exp.h
DOMAIN=DUCT2500                          # See definitions in scr/Harmonie_domains.pm
TOPO_SOURCE=gmted2010                    # Input source for orography.
GRID_TYPE=CUBIC                          # Type of grid (LINEAR|QUADRATIC|CUBIC)
VLEV=65                                  # Vertical level definition name

# In harmonie_exp/scr/Harmonie_domains.pm
sub Harmonie_domains{
  my $domain=shift;
  my %domains = (
 'DUCT750'=>{
      'TSTEP'  => '30',
      'NLON'   => '800',
      'NLAT'   => '720',
      'LONC'   => '21.38',
      'LATC'   => '59.78',
      'LON0'   => '21.38',
      'LAT0'   => '59.78',
      'GSIZE'  => '750.',
    },
 'DUCT2500'=>{
      'TSTEP'  => '60',
      'NLON'   => '400',
      'NLAT'   => '360',
      'LONC'   => '21.38',
      'LATC'   => '59.78',
      'LON0'   => '21.38',
      'LAT0'   => '59.78',
      'GSIZE'  => '2500.',
    },
```

https://doi.org/10.5194/egusphere-2026-1629
Preprint. Discussion started: 22 May 2026

For reasons of national security, the computational code used for ducting calculations is not available. However, pre-computed modified refractive values based on point forecasts for the Utö measurement station, along with observations for the test period (19 June 2022 – 11 July 2022), are made available. These datasets are provided in NetCDF and csv format and can be accessed for further analysis: DOI10.5281/zenodo.20305838 (Hämäläinen et al., 2026).

All scripts for plotting are available: https://zenodo.org/records/20305839 (Hämäläinen, 2026).

Author contributions. Karoliina Hämäläinen: Model simulations, Data analysis, Writing (main responsible for draft preparation and editing). Laura Rautiainen: Providing observational data, Writing (review, editing). Jani Tyynelä: Supervision, Writing (review, editing), Project administration. Lauri Laakso: Supervision, Writing (review)

Competing interests. The authors declare that they have no financial, personal, or other competing interests that could have influenced the work reported in this paper.

Acknowledgements. The authors gratefully acknowledge the Finnish Scientific Advisory Board for Defence for funding this research through the project *"Predicting signal propagation conditions using numerical methods"*. In addition, a preliminary study supporting this work was funded by the Academy of Finland through the project *"Enabling forecasts on radar performance in marine environment"* (project number 338150).

The authors also acknowledge the technical and research infrastructure support provided by the Finnish Marine Research Infrastructure (FINMARI) and the Integrated Carbon Observing System (ICOS), which contributed to the data collection and analysis used in this study. The authors further acknowledge the ACCORD consortium for the development and continued advancement of the Harmonie-AROME modelling system.

https://doi.org/10.5194/egusphere-2026-1629
Preprint. Discussion started: 22 May 2026

References

Ao, C. O.: Effect of ducting on radio occultation measurements: An assessment based on high-resolution radiosonde soundings, Radio Science, 42, 1–15, https://doi.org/10.1029/2006RS003485, 2007.

Babin, S. M., Young, G. S., and Carton, J. A.: A new model of the oceanic evaporation duct, Journal of Applied Meteorology and Climatology, 36, 193–204, 1997.

Barkmeijer, J., Lindskog, M., Gustafsson, N., Bojarova, J., Azad, R., Monteiro, I., Secriba, P., Whelan, E., Ridal, M., Sánchez Arriola, J., et al.: HARMONIE-AROME 4D-Var, ALADIN-HIRLAM Newsletter No. 16, https://www.umr-cnrm.fr/aladin/IMG/pdf/nl16.pdf, published February 8, 2021, 2021.

Bechtold, P.: Atmospheric Thermodynamics, Tech. rep., ECMWF, Shinfield Park, Reading, England, https://www.ecmwf.int/sites/default/files/elibrary/2015/16954-atmospheric-thermodynamics.pdf, accessed: 2023-03-02, 2015.

Bengtsson, L., Andrae, U., Aspelien, T., Batrak, Y., Calvo, J., de Rooy, W., Gleeson, E., Hansen-Sass, B., Homleid, M., Hortal, M., et al.: The HARMONIE–AROME model configuration in the ALADIN–HIRLAM NWP system, Monthly Weather Review, 145, 1919–1935, 2017.

Bubnová, R., Hello, G., Bénard, P., and Geleyn, J.-F.: Integration of the Fully Elastic Equations Cast in the Hydrostatic Pressure Terrain-Following Coordinate in the Framework of the ARPEGE/Aladin NWP System, Monthly Weather Review, 123, 515–535, https://doi.org/10.1175/1520-0493(1995)123<0515:IOTFEE>2.0.CO;2, 1995.

Bénard, P., Vivoda, J., Mašek, J., Smolíková, P., Yessad, K., Smith, C., Brožková, R., and Geleyn, J.-F.: Dynamical kernel of the Aladin–NH spectral limited-area model: Revised formulation and sensitivity experiments, Quarterly Journal of the Royal Meteorological Society, 136, 155–169, https://doi.org/10.1002/qj.522, 2010.

Derksen, J.: Radar Performance Modelling, Master's thesis, Delft University of Technology, 2016.

Dian, M. and Masek, J.: Improving the Computation of Screen Level Fields (Temperature, Moisture), Report of LACE Stay at CHMI in Prague 11.04. 2015–29.04. 2015, 2015, Prague, https://www.rclace.eu/media/files/Physics/2016/dian_screeninter_pragueApr2016.pdf, 2015.

ECMWF: IFS Documentation CY41R1: Part III: Dynamics and Numerical Procedures, ECMWF, https://www.ecmwf.int/node/9210, accessed: 2015-03-02, 2015.

ECMWF: IFS Documentation, https://www.ecmwf.int/en/publications/ifs-documentation, accessed: 2023-03-14, 2023.

Essen, H., Danklmayer, A., Förster, J., Behn, M., Hurtaud, Y., Fabbro, V., and Castanet, L.: Joint French-German radar measurements for the determination of the refractive index in the maritime boundary layer, in: Optics in Atmospheric Propagation and Adaptive Systems XV, vol. 8535, pp. 16–24, SPIE, 2012.

Förster, J. and Riechen, J.: Measurements of refractive variability in the marine boundary layer in comparison with mesoscale meteorological model predictions, in: Optics in atmospheric propagation and adaptive systems IX, vol. 6364, p. 636402, SPIE, 2006.

Frogner, I.-L., Andrae, U., Bojarova, J., Callado, A., Escribà, P., Feddersen, H., Hally, A., Kauhanen, J., Randriamampianina, R., Singleton, A., et al.: HarmonEPS—the HARMONIE ensemble prediction system, Weather and Forecasting, 34, 1909–1937, 2019.

Geleyn, J.-F.: Interpolation of wind, temperature and humidity values from model levels to the height of measurement, Tellus A, 40, 347–351, 1988.

https://doi.org/10.5194/egusphere-2026-1629
Preprint. Discussion started: 22 May 2026

Good, S., Fiedler, E., Mao, C., Martin, M. J., Maycock, A., Reid, R., Roberts-Jones, J., Searle, T., Waters, J., While, J., et al.: The current configuration of the OSTIA system for operational production of foundation sea surface temperature and ice concentration analyses, Remote Sensing, 12, 720, 2020.

Grabner, M. and Kvicera, V.: Refractive index measurement at TV tower Prague, RADIOENGINEERING-PRAGUE-, 12, 5–7, 2003.

Grønsleth, M. S. and Randriamampianina, R.: Assimilation of Radar Reflectivity Data in HARMONIE, Tech. rep., Norwegian Meteorological Institute, https://www.researchgate.net/profile/Roger-Randriamampianina/publication/265360510_Assimilation_of_radar_reflectivity_data_in_HARMONIE/links/54c651dd0cf2911c7a58aa76/Assimilation-of-radar-reflectivity-data-in-HARMONIE.pdf, accessed: 2023-03-19, 2012.

Haack, T., Wang, C., Garrett, S., Glazer, A., Mailhot, J., and Marshall, R.: Mesoscale modeling of boundary layer refractivity and atmospheric ducting, Journal of applied meteorology and climatology, 49, 2437–2457, 2010.

Hagelin, S., Azad, R., Lindskog, M., Schyberg, H., and Körnich, H.: Evaluating the use of Aeolus satellite observations in the regional numerical weather prediction (NWP) model Harmonie-Arome, Atmospheric Measurement Techniques, 14, 5925–5938, 2021.

Hämäläinen, K.: Harmonie-AROME ducting plotting, https://zenodo.org/records/20305839, 2026.

Hämäläinen, K., Rautiainen, L., Tyynelä, J., and Laakso, L.: Data for manuscript: "Effects of model resolution on predicting atmospheric ducting conditions with Harmonie-AROME", https://doi.org/https://doi.org/10.5281/zenodo.20305838, 2026.

Honkanen, M., Tuovinen, J.-P., Laurila, T., Mäkelä, T., Hatakka, J., Kielosto, S., and Laakso, L.: Measuring turbulent CO2 fluxes with a closed-path gas analyzer in a marine environment, Atmos. Meas. Tech., 11, 5335–5350, https://doi.org/10.5194/amt-11-5335-2018, 2018.

Laakso, L., Mikkonen, S., Drebs, A., Karjalainen, A., Pirinen, P., and Alenius, P.: 100 years of atmospheric and marine observations at the Finnish Utö Island in the Baltic Sea, Ocean science, 14, 617–632, 2018.

Laprise, R.: The Euler Equations of Motion with Hydrostatic Pressure as an Independent Variable, Monthly Weather Review, 120, 197–207, https://doi.org/10.1175/1520-0493(1992)120<0197:TEEOMW>2.0.CO;2, 1992.

Lenderink, G. and Holtslag, A. A.: An updated length-scale formulation for turbulent mixing in clear and cloudy boundary layers, Quarterly Journal of the Royal Meteorological Society: A journal of the atmospheric sciences, applied meteorology and physical oceanography, 130, 3405–3427, 2004.

Lopez, P.: A 5-yr 40-km-resolution global climatology of superrefraction for ground-based weather radars, Journal of applied meteorology and climatology, 48, 89–110, 2009.

Mai, Y., Sheng, Z., Shi, H., Liao, Q., and Zhang, W.: Spatiotemporal distribution of atmospheric ducts in Alaska and its relationship with the Arctic vortex, International Journal of Antennas and Propagation, 2020, 9673 289, 2020.

Mesnard, F. and Sauvageot, H.: Climatology of anomalous propagation radar echoes in a coastal area, Journal of Applied Meteorology and Climatology, 49, 2285–2300, 2010.

Müller, M., Homleid, M., Ivarsson, K.-I., Køltzow, M. A., Lindskog, M., Midtbø, K. H., Andrae, U., Aspelien, T., Berggren, L., Bjørge, D., et al.: AROME-MetCoOp: A Nordic convective-scale operational weather prediction model, Weather and Forecasting, 32, 609–627, 2017.

Norin, L.: Observations of anomalous propagation over waters near Sweden, Atmospheric Measurement Techniques Discussions, 2022, 1–20, 2022.

Norin, L., Wellander, N., and Devasthale, A.: Anomalous propagation and the sinking of the Russian warship Moskva, Bulletin of the American Meteorological Society, 104, E2286–E2304, 2023.

Pastore, D. M., Greenway, D. P., Stanek, M. J., Wessinger, S. E., Haack, T., Wang, Q., and Hackett, E. E.: Comparison of atmospheric refractivity estimation methods and their influence on radar propagation predictions, Radio Science, 56, 1–17, 2021.

https://doi.org/10.5194/egusphere-2026-1629
Preprint. Discussion started: 22 May 2026

Patterson, W. L. and Skolnik, M.: The Propagation Factor, Fp, in the radar equation, Radar Handbook, p. 263, 2008.

Rautiainen, L., Tyynelä, J., Lensu, M., Siiriä, S., Vakkari, V., O'Connor, E., Hämäläinen, K., Lonka, H., Stenbäck, K., Koistinen, J., et al.: Utö Observatory for Analysing Atmospheric Ducting Events over Baltic Coastal and Marine Waters, Remote Sensing, 15, 2989, 2023a.

Rautiainen, L., Tyynelä, J., and Laakso, L.: Occurrence and characteristics of ducts based on radiosonde profiles measured at Jokioinen., Tech. rep., Finnish Meteorological Institute, 2023b.

Rautiainen, L., Lensu, M., Vakkari, V., Tyynelä, J., Kanarik, H., and Laakso, L.: Marine Atmospheric Ducting Statistics Based on 2 Years of Coastal Surveillance Radar Observations, Journal of Applied Meteorology and Climatology, 64, 63–76, 2025.

Seity, Y., Brousseau, P., Malardel, S., Hello, G., Bénard, P., Bouttier, F., Lac, C., and Masson, V.: The AROME-France convective-scale operational model, Monthly Weather Review, 139, 976–991, 2011.

Simmons, A. J. and Burridge, D. M.: An Energy and Angular-Momentum Conserving Vertical Finite-Difference Scheme and Hybrid Vertical Coordinates, Monthly Weather Review, 109, 758–766, https://doi.org/10.1175/1520-0493(1981)109<0758:AEAAMC>2.0.CO;2, 1981.

Turton, J., Bennetts, D., and Farmer, S. G.: An introduction to radio ducting, Meteorological Magazine, 117, 245–254, 1988.

Van Meijgaard, E., Van Ulft, L., Lenderink, G., De Roode, S., Wipfler, E. L., Boers, R., and van Timmermans, R.: Refinement and application of a regional atmospheric model for climate scenario calculations of Western Europe, KVR 054/12, KVR, 2012.

Von Engeln, A. and Teixeira, J.: A ducting climatology derived from the European Centre for Medium-Range Weather Forecasts global analysis fields, Journal of Geophysical Research: Atmospheres, 109, 2004.

Wagner, N. K.: An analysis of radiosonde effects on the measured frequency of occurrence of ducting layers, Journal of Geophysical Research, 65, 2077–2085, 1960.

https://doi.org/10.5194/egusphere-2026-1629
Preprint. Discussion started: 22 May 2026

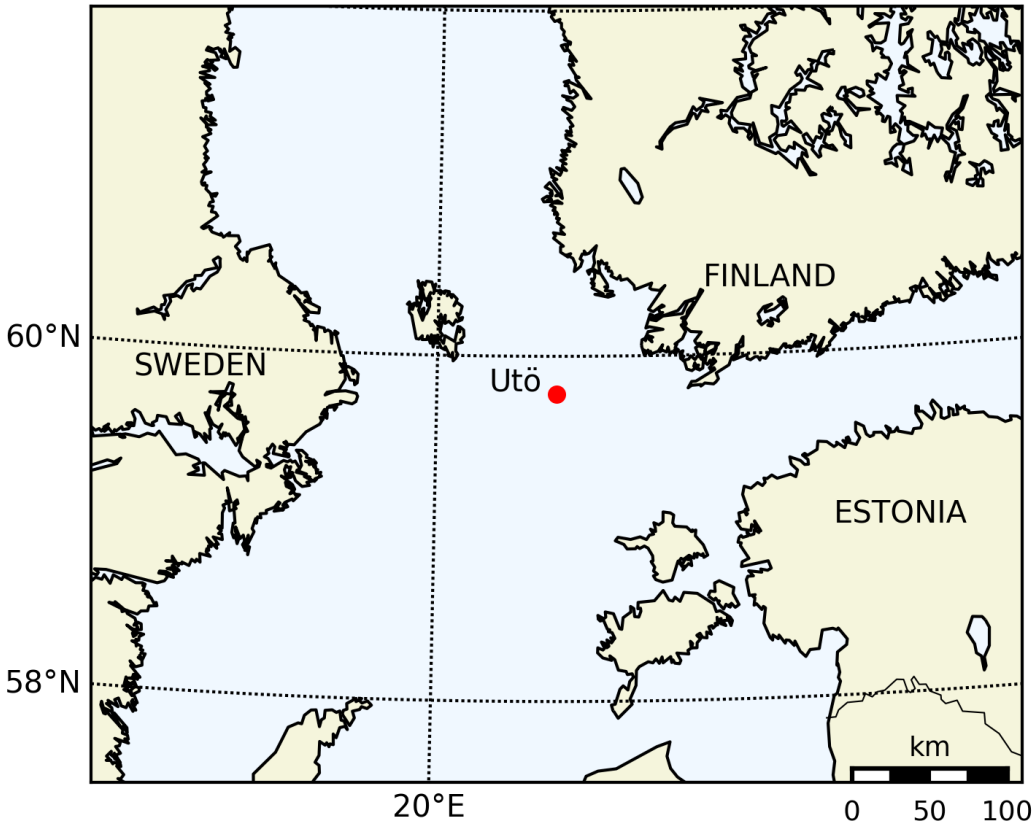

Figure 1. Model domain around Utö Island in the southwest Finnish archipelago. Utö Island is marked with a red dot.

https://doi.org/10.5194/egusphere-2026-1629
Preprint. Discussion started: 22 May 2026

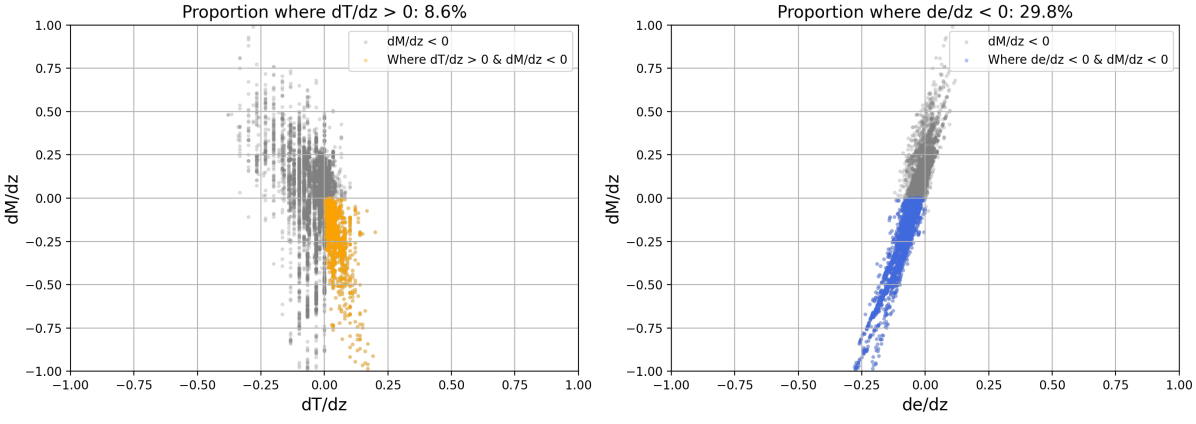

Figure 2. Scatter plots of temperature (dT/dh, orange) and water vapor pressure (de/dh, blue) gradients versus the modified refractivity gradient (dM/dh, gray) at different vertical levels, based on observations. The proportion of cases are given in the titles.

https://doi.org/10.5194/egusphere-2026-1629
Preprint. Discussion started: 22 May 2026

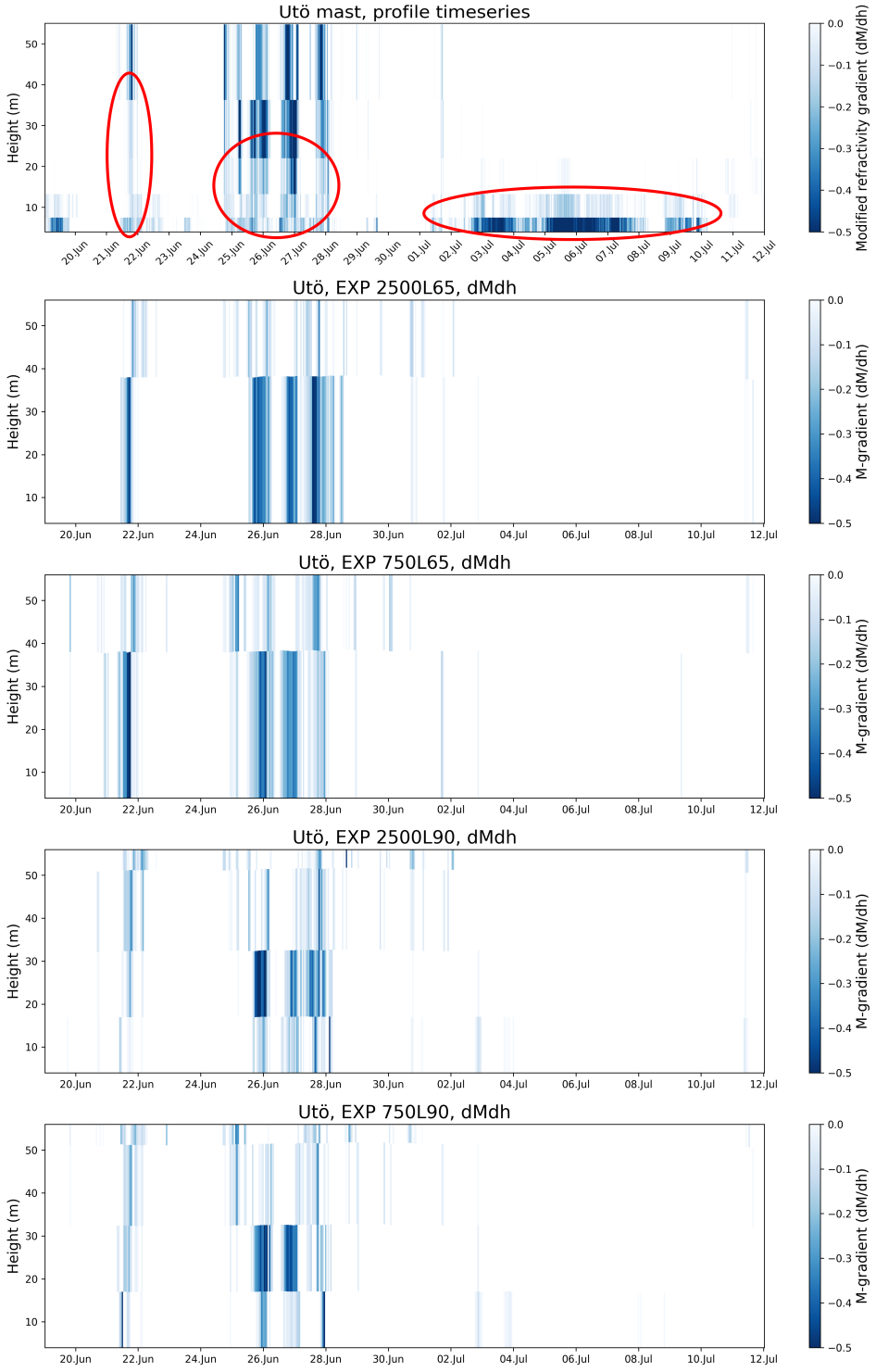

Figure 3. Modified refractivity gradient from Utö mast measurements and four HARMONIE-AROME model simulations during 19 June–11 July 2022. Negative values (blue) indicate potential ducting.

https://doi.org/10.5194/egusphere-2026-1629
Preprint. Discussion started: 22 May 2026

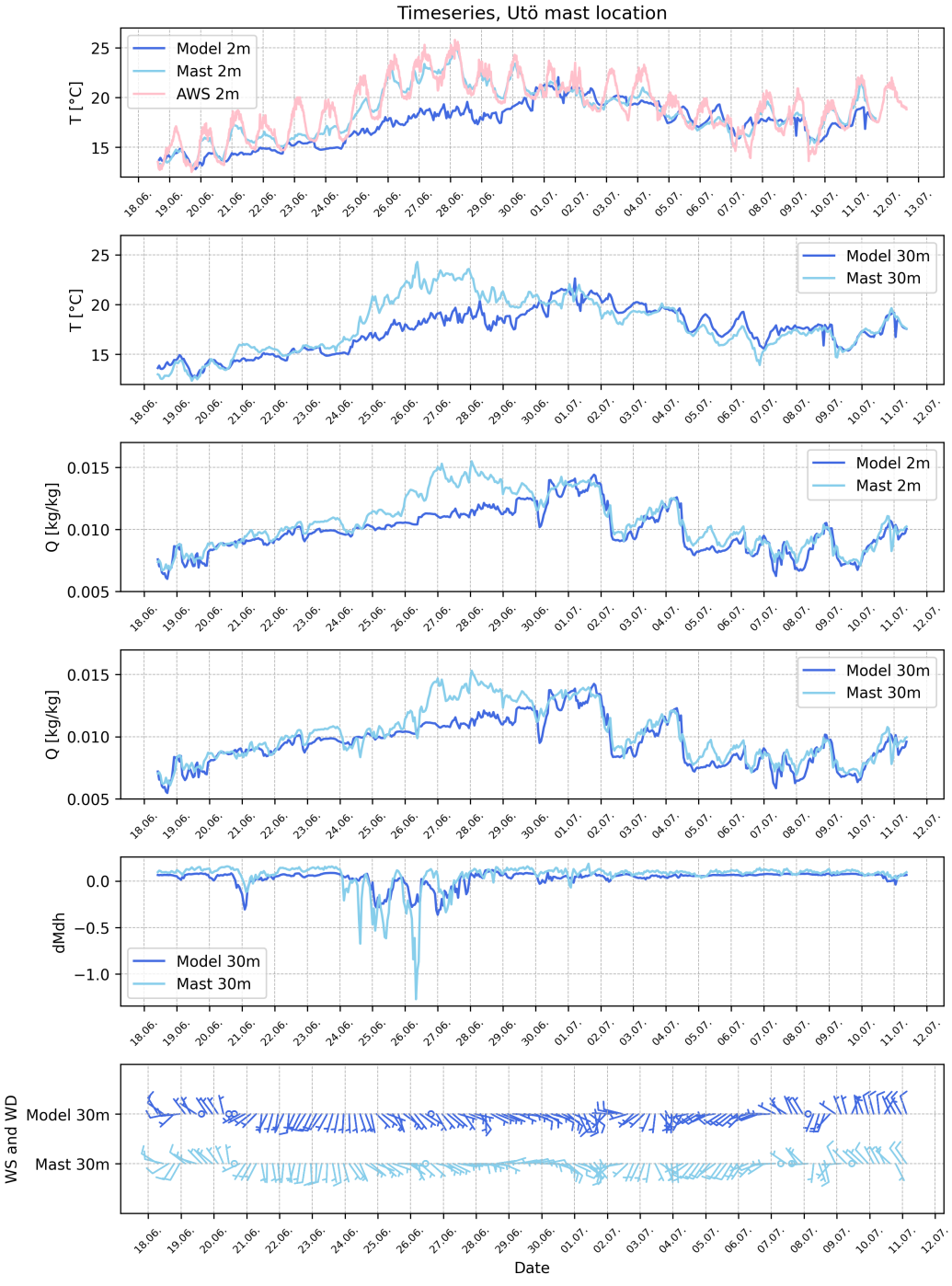

Figure 4. Time series of temperature (T), specific humidity (Q), modified refractivity gradient (dM/dh), and wind speed (WS) and direction (WD) at 2 m and 30 m. Dark blue curves show the operational model configuration, light blue curves show observations from the Utö mast, and the pink curve in the top panel represents temperature from the nearest Automatic Weather Station (AWS) located further inland on Utö Island.

https://doi.org/10.5194/egusphere-2026-1629
Preprint. Discussion started: 22 May 2026

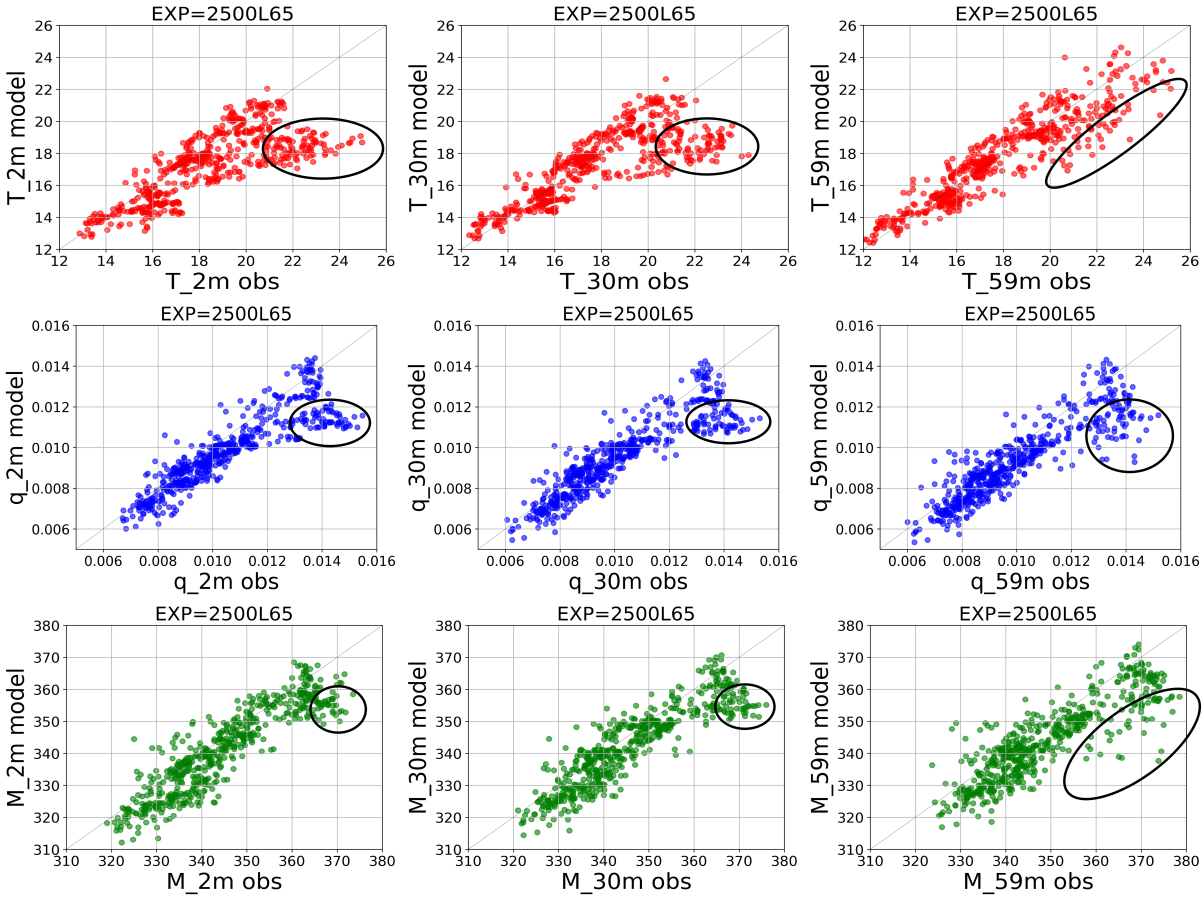

Figure 5. Scatter plots of temperature (T, red), specific humidity (q, blue), and modified refractivity (M, green) at 2 m, 30 m, and 59 m. Model values (y-axis) are plotted against observations (x-axis).

https://doi.org/10.5194/egusphere-2026-1629
Preprint. Discussion started: 22 May 2026

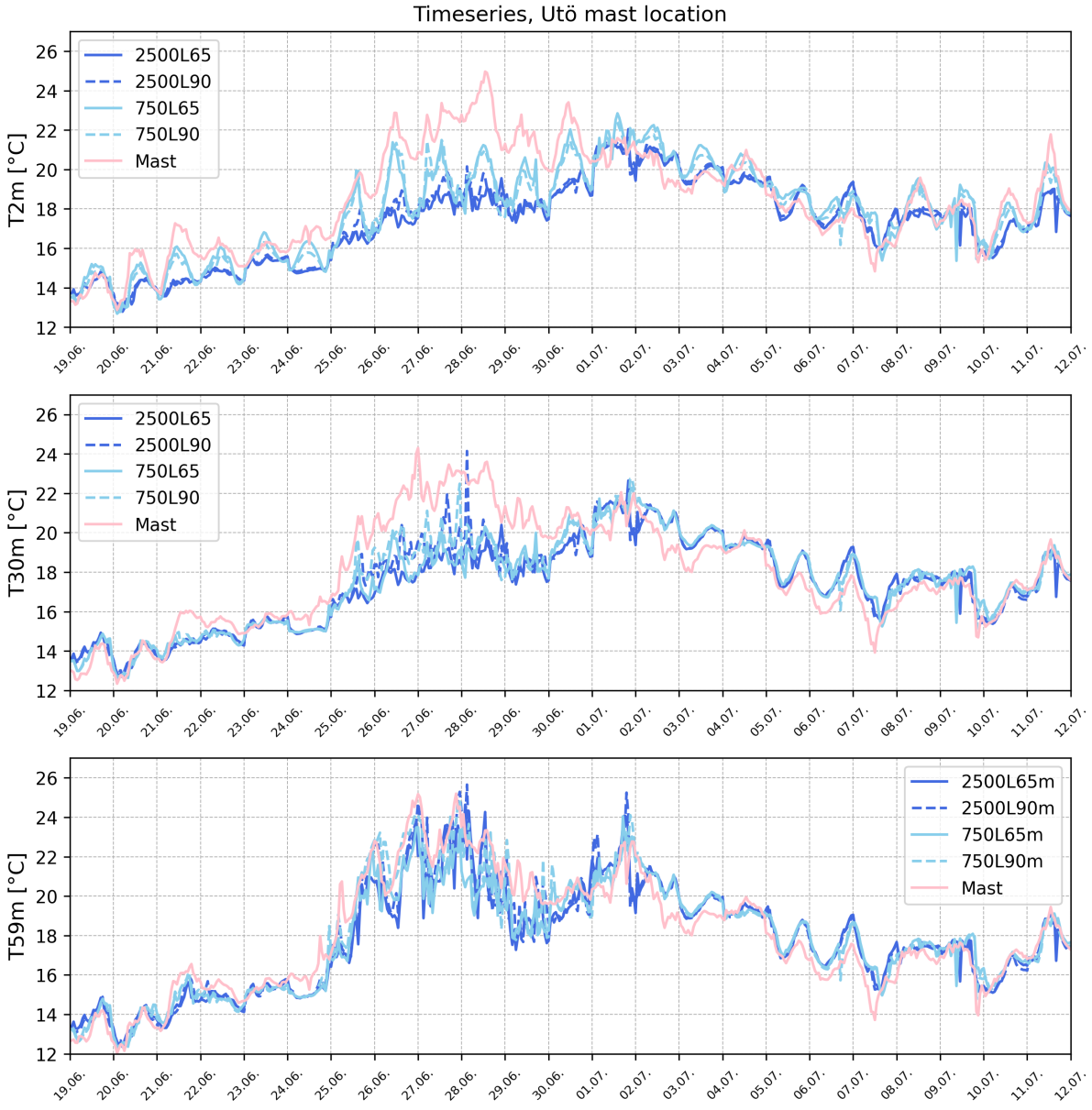

Figure 6. Time series of temperature at three levels: 2 m (top), 30 m (middle), and 59 m (bottom). Colors indicate horizontal resolutions of 2500 m (dark blue) and 750 m (light blue), with observations in pink. Vertical resolutions are shown by solid lines (65 levels) and dashed lines (90 levels).

https://doi.org/10.5194/egusphere-2026-1629
Preprint. Discussion started: 22 May 2026

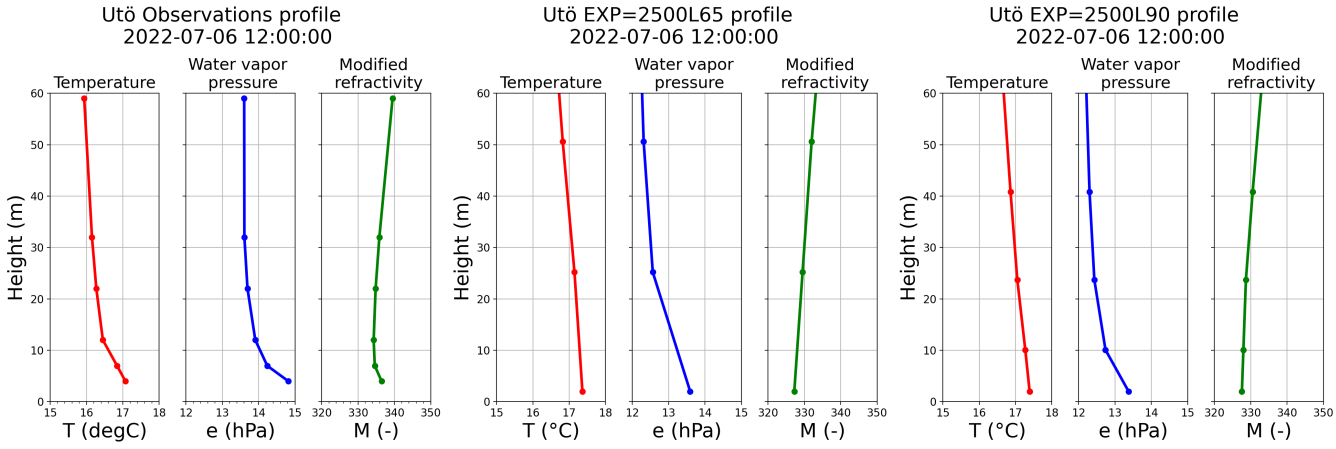

Figure 7. Vertical profiles on 6 July 2022 at 12 UTC from the Utö mast and two model configurations with different numbers of levels (2500L65 and 2500L90). Colors indicate temperature (T, red), water vapor pressure (e, blue), and modified refractivity (M, green).

https://doi.org/10.5194/egusphere-2026-1629
Preprint. Discussion started: 22 May 2026

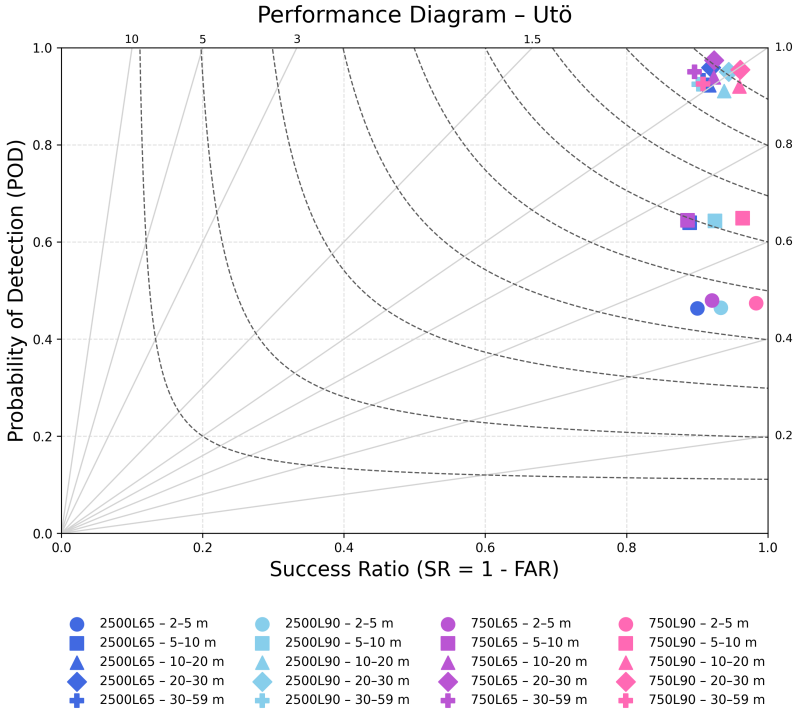

Figure 8. Performance diagram of modeled modified refractivity against Utö mast measurements, showing four skill scores: POD (vertical axis), success ratio (horizontal axis), frequency bias (Bias, straight lines), and threat score (TS, curved lines). Model experiments are distinguished by color, with symbols indicate heights. The perfect score lies at the top-right corner. All forecast lead times (+1 to +24 h) are included.

https://doi.org/10.5194/egusphere-2026-1629
Preprint. Discussion started: 22 May 2026

Table 1. Effects of temperature and humidity on strength of refractivity, N.

Temperature	Humidity	Duct strength
Warm	Dry	+
Warm	Humid	++
Cold	Dry	+++
Cold	Humid	++++

https://doi.org/10.5194/egusphere-2026-1629
Preprint. Discussion started: 22 May 2026

Table 2. List of different model set-ups.

Experiment	Horizontal resolution	Number of model levels
750L65	750m	65
2500L65	2500m	65
750L90	750m	90
2500L90	2500m	90